Impact of the Acidic C-Terminal Region Comprising Amino Acids 109−140 on α-Synuclein Aggregation in Vitro†

Wolfgang Hoyer,‡ Dmitry Cherny,‡,§ Vinod Subramaniam,*,‡,|| and Thomas M. Jovin*,‡

Department of Molecular Biology, Max Planck Institute for Biophysical Chemistry, Am Fassberg 11, D-37077 Goettingen, Germany, Institute of Molecular Genetics, Russian Academy of Sciences, Kurchatov's Square, 123182 Moscow, Russia, and Biophysical Engineering Group, Faculty of Science and Technology, University of Twente, P.O. Box 217, 7500 AE Enschede, The Netherlands

Received July 20, 2004; Revised Manuscript Received September 16, 2004

ABSTRACT: The aggregation of α-synuclein, involved in the pathogenesis of several neurodegenerative disorders such as Parkinson's disease, is enhanced in vitro by biogenic polyamines binding to the highly charged C-terminal region aa109−140. In this study, we investigated the influence of this region on the aggregation kinetics, monitored by thioflavin T binding and static light scattering, and morphology, assessed by electron microscopy, fluorescence microscopy, and turbidity, by comparing the effect of various solution conditions on the wild-type protein, the disease related mutants A53T and A30P, and two truncated variants, syn(1−108) and syn(1−124), lacking the complete or the C-terminal half of the polyamine binding site. In the presence of the intact C-terminus, aggregation was strongly retarded in physiological buffer. This inhibition of aggregation was overridden by (i) addition of spermine or $MgCl_2$ or lowering of pH, leading to strong charge shielding in the C-terminus or (ii) by truncation of aa125−140 or aa109−140. Addition of $MgCl_2$ or spermine or acidification were not effective in promoting aggregation of syn(1−108). The impact of the disease-related mutations on the aggregation kinetics was dependent on the solution conditions, with the aggregation propensity order A53T ∼ wt > A30P at low ionic strength, but A53T > wt ∼ A30P at high ionic strength, with exceedingly potent promotion of aggregation by the A53T mutation in the presence of spermine. In contrast to full-length α-synuclein aggregates, those formed from syn(1−108) did not exhibit a pronounced polymorphism. The effects of the C-terminus on aggregation cannot be rationalized merely by a contribution to the protein net charge, but rather suggest a specific role of aa109−140 in the regulation of aggregation, presumably involving formation of intramolecular contacts.

The intracellular deposition of insoluble α-synuclein is associated with Parkinson's disease (PD)[1] and other neurodegenerative diseases (synucleinopathies), such as dementia with Lewy bodies and multiple system atrophy (*1*−*5*). α-Synuclein constitutes the major component of Lewy bodies and Lewy neurites, cytoplasmic inclusions of fibrillar and granular material that define PD neuropathologically (*3*). The importance of α-synuclein in the etiology of PD is highlighted by two missense mutations in the α-synuclein gene (A30P, A53T) which have been linked to early-onset, familial PD (*6*, *7*).

α-Synuclein is classified as a natively unfolded protein, since it exhibits a random-coil secondary structure in vitro in physiological buffers (*8*). Upon incubation at elevated temperature, a transition in secondary structure toward a high β-sheet content occurs, resulting in protein aggregates that share the characteristic features of amyloid and resemble proteinaceous material isolated from disease-affected brain (*9*−*12*). The kinetics of the aggregation process is in agreement with a nucleation−polymerization model exhibiting an initial lag phase followed by aggregate growth (*13*, *14*). The rates of nucleation and aggregate growth are highly sensitive to the incubation conditions, e.g., the solution pH (*15*, *16*). A wide variety of molecules could have been identified that accelerate α-synuclein aggregation in vitro, pointing toward a link between conformational and ligand binding flexibility. Positively charged molecules constitute a particularly potent class of aggregation promoters. In addition to metal cations (*15*, *17*−*20*), polycations such as cellular polyamines strongly accelerate α-synuclein aggregation, suggesting a possible role of these compounds in the etiology of the synucleinopathies (*14*, *21*, *22*).

In addition to the kinetics of aggregation, aggregate morphology is highly dependent on the incubation conditions. Annular and tubular structures are detected in protofibrillar fractions (*23*−*26*). The typical mature amyloid fibril represents a major end product of aggregation, but large amorphous aggregates constitute a second possible outcome,

† W.H. was the recipient of a fellowship from the Stiftung Stipendien-Fonds des Verbandes der Chemischen Industrie and the Bundesministerium für Bildung und Forschung.

* Corresponding authors. T.M.J.: Tel, +49 551 2011382; Fax, +49 551 2011467; e-mail, tjovin@gwdg.de. V.S.: Tel, +31 53 4893157; Fax, +31 53 4891105; e-mail, V.Subramaniam@tnw.utwente.nl.

‡ Max Planck Institute for Biophysical Chemistry.

§ Russian Academy of Sciences.

|| University of Twente.

[1] Abbreviations: aa, amino acids; CD, circular dichroism; ESI-MS, electrospray ionization mass spectrometry; MES, 2-(*N*-morpholino)-ethanesulfonic acid; PD, Parkinson's disease; ThioT, thioflavin T; wt, wild-type.

10.1021/bi048453u CCC: $27.50
Published on Web 11/26/2004

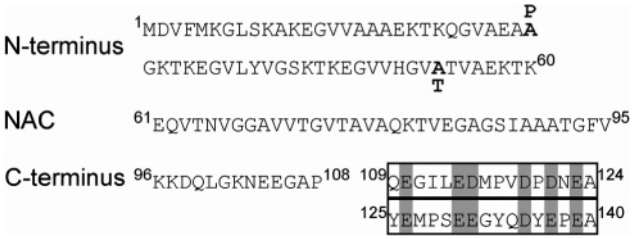

FIGURE 1: Primary sequence and domains of α-synuclein. The acidic residues in the tandem repeat comprising the polyamine binding site, region aa109−140, are aligned and highlighted in gray. The disease-related point mutations, A30P and A53T, are in bold.

depending on the incubation conditions, e.g., pH and salt concentration (*15*). However, an unambiguous discrimination between fibrillar and amorphous aggregates is not feasible inasmuch as amorphous aggregates can contain fibrillar material and share the staining properties of amyloid fibrils (*15*).

The primary sequence of human α-synuclein (140 aa) can be subdivided into three distinct regions (Figure 1): The N-terminal region (residues 1−60) comprises both mutation sites associated with familial PD. It covers the majority of the six imperfect 11 amino acid repeats with a highly conserved hexamer motif KTKEGV (residues 1−87), which assume α-helical structure when associated with phospholipid membranes (*27*, *28*). The central region (residues 61−95), also denoted NAC, is highly hydrophobic and essential for aggregation (*29*, *30*).

The C-terminal region (residues 96−140) is very acidic, containing 10 glutamate and five aspartate residues. It is responsible for the high thermostability (*31*) and is essential for the chaperone function (*20*, *32*−*34*) of α-synuclein by serving as a solubilizing domain. Moreover, it regulates amyloid aggregation, since C-terminally truncated fragments aggregate faster than the full-length protein (*11*, *35*, *36*) and post-translational modifications, e.g., phosphorylation, of C-terminal amino acids modulate the aggregation propensity (*37*, *38*). Despite its modulating effect on aggregation, the C-terminus is not incorporated into the core structure of α-synuclein fibrils but is located on their surface (*39*−*41*).

Due to its acidic nature, the C-terminus is a likely candidate for interaction with cationic compounds. Specific binding to the C-terminus was demonstrated for Ca^{2+} and Cu^{2+} (*18*, *19*). Recently, a well-defined polyamine binding interface (region aa109−140) was identified in the C-terminal domain by NMR (*14*). Polyamine binding to the monomeric protein did not induce secondary structure changes detectable by circular dichroism (CD) or NMR spectroscopy but correlated with the enhancement of aggregation (*14*). The region aa109−140 also corresponds to the domain involved in Ca^{2+} binding (*19*), implying that this region might be the primary interface for interaction with cationic compounds. The acidic residues in this 32aa region are organized as a tandem repeat of 16 residues (Figure 1). Interestingly, the C-terminus is not essential for maintaining the unfolded nature of α-synuclein (*34*).

The involvement of the A30P and A53T mutations in familial PD has stimulated comparative studies of the aggregation kinetics of the wild-type and the mutant proteins. These studies have consistently reported an aggregation-promoting effect of the A53T mutation (*11*, *23*, *42*−*44*). In contrast, the results for the A30P mutation are inconclusive, in as much as they have reported either faster aggregation of the mutant protein (*43*), identical speed of aggregation (*11*), or slower fibrillation but faster monomer consumption of the mutant protein compared to wild-type α-synuclein (*23*, *42*, *44*).

In this study we investigated the influence of the C-terminus, specifically residues 109−140, and the disease-related mutations on α-synuclein aggregation by monitoring the aggregation kinetics and by imaging the aggregates of wild-type α-synuclein, the A30P and A53T mutants, as well as the C-terminally truncated variants of the wild-type protein comprising the amino acid residues 1−124 [syn(1−124)] and 1−108 [syn(1−108)], respectively. Syn(1−124) is missing one and syn(1−108) both of the tandem repeats indicated in Figure 1.

EXPERIMENTAL PROCEDURES

Preparation of Wild-Type, Mutant, and Truncated α-Synuclein. Recombinant human wild-type, A53T, and A30P α-synuclein were expressed and purified as described (*15*) using plasmid pT7−7 encoding for the proteins (courtesy of the Lansbury laboratory, Harvard Medical School, Cambridge, MA). The carboxy-terminally truncated wild-type α-synuclein fragments syn(1−108) and syn(1−124) were amplified by PCR from full-length wild-type α-synuclein and subcloned into pT7−7. The sequences were validated by DNA sequencing. Expression and purification of the truncated proteins was performed essentially as described for full-length α-synuclein (*15*). The identity of all proteins was verified by ESI-MS. Protein concentrations were determined with the bicinchoninic acid (BCA) assay and validated by absorbance measurements at 275 nm using an extinction coefficient of 1400 M^{-1} cm^{-1} per tyrosine residue. Net charges and pIs were calculated using pK_a values from ref *45*.

α-Synuclein Aggregation. Amyloid formation was followed in triplicates of 300 μL samples of freshly prepared 100 μM α-synuclein solutions in 25 mM Tris-HCl, pH 7.5 (at 37 °C), without any additions or with addition of either 150 mM NaCl, 0.3 mM spermine, 3 mM spermine, or 10 mM $MgCl_2$. Fibril formation was also followed in 50 mM Na-acetate, pH 4.0 (at 37 °C), in the absence of additives. The solutions were incubated in glass vials at 37 °C and stirred with micro stir bars using a multiple drive stirrer (Telesystem HP15S, Variomag) at 300 rpm. Aliquots were withdrawn during the course of the incubations and analyzed by either ThioT binding or static light scattering. For ThioT binding, 2.0 mL of 5 μM ThioT in either 50 mM Na-glycinate, pH 8.2 (pH 7.5 incubations), or 50 mM Na-MES, pH 6.0 (pH 4.0 incubations), was added to a 7.5 μL aliquot of the respective incubation. The final protein concentration was 0.37 μM. Fluorescence measurements were carried out as described earlier (*15*). For static light scattering measurements, 56 μL of 25 mM Tris-HCl, pH 7.5, was added to 4 μL aliquots of the respective incubation. The intensity of scattered light was measured at a wavelength of 340 nm and an angle of 90° with a Cary Eclipse spectrofluorimeter (Varian) using quartz microcuvettes with a 0.3 cm light-path (Hellma). Excitation and emission bandwidths were 5 nm.

Evaluation of Kinetic Data. Kinetic traces were generated from time points of ThioT emission or static light scattering, respectively. The data were fit with the commercial program Kaleidagraph (Synergy Software) to the equation

$$\alpha[t] = \frac{1 - e^{-k_{app}t}}{1 + ae^{-k_{app}t}} \cong \frac{1 - e^{-k_{app}t}}{1 + e^{-k_{app}(t-t_{1/2})}}$$
$$(\alpha[t_{1/2}] = 1/2 \text{ to a very good approximation}) \quad (1)$$

which is derived from a simple kinetic model introduced in ref *14*. The model assumes an initial formation of nucleation centers at very low concentration according to a dynamic mass−action equilibrium, aggregate growth by the addition of monomers to the aggregates, and evolution of growth centers by amorphous aggregation and/or mechanical fragmentation of aggregates. Aggregate growth is characterized by the rate constant k_{app}, whereas the nucleation events are reflected in the constant *a*, with smaller values of *a* corresponding to facilitated nucleation. Each experimental time trace was fit individually and normalized to $\alpha[\infty] = 1$. Normalization was required as the final fluorescence emission intensities differed for the various solution compositions, presumably reflecting differences in the aggregate morphologies, the chemical properties of aggregate surfaces, and/or the environmental conditions (*15*), but not primarily the fractional conversion of monomer. The latter was >85% for all solution conditions, as determined for the full-length wild-type and truncated syn(1−108) protein by measuring the protein concentration in the supernatant after centrifugation of aggregated solutions at 100000*g* (Beckman Airfuge). A mean fit for each triplicate set was calculated as the average of the three fits in the inverted form of eq 1.

Circular Dichroism (CD) Measurements. Far-UV CD measurements were performed on a Jasco J720 spectropolarimeter using a protein concentration of 78 μM in either 25 mM Tris-HCl, pH 7.5, or 50 mM Na-acetate, pH 4.0. Spectra were recorded from 195 to 260 nm in a 0.01 cm path length cuvette. Twenty scans were averaged without smoothing and corrected for the buffer spectrum. CD measurements were done in triplicate and averaged.

Turbidity Measurements. A 10 μL portion of the α-synuclein incubations were added to 75 μL of either 25 mM Tris-HCl, pH 7.5 (pH 7.5 incubations), or 50 mM Na-acetate, pH 4.0 (pH 4.0 incubations). The final protein concentration was 12 μM. As a measure of turbidity, the absorbance at 340 nm was determined in a 1 cm path length microcuvette (Hellma) in a Cary 100 Spectrophotometer (Varian).

Electron Microscopy. An aliquot was withdrawn from the incubation mixture and placed on a glow-discharged carbon film attached to an EM grid. Carbon films, 3−4 nm thick, were pretreated by glow discharge in the presence of pentylamine vapor (residual pressure ~150 milliTorr, discharge current 2−3 mA, duration of discharge 30 s) as described elsewhere (*46*). The adsorption continued for 1−2 min, after which the grids were rinsed with a few drops of 2% aqueous uranyl acetate, blotted with filter paper, and dried. The samples were examined with a Philips CM12 electron microscope (Philips). The negatives were scanned with a DuoScan T2500 scanner (Agfa) at 1200 dpi. Measurements of the micrographs were carried out with the Windows version of NIH Image (Scion Corp.). For printing, images were flattened using a high-pass filter with a radius of 250 pixels and subsequently adjusted for contrast/brightness using Adobe Photoshop.

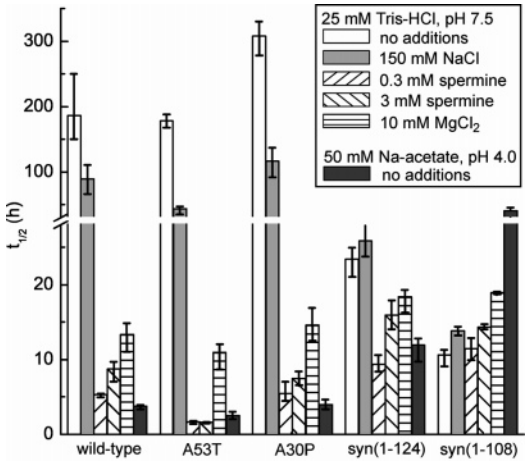

FIGURE 2: Aggregation half-times $t_{1/2}$ for each construct/condition. Averages of $t_{1/2}$ (incubation time required for ThioT fluorescence or light scattering to reach 50% of the final intensity) are given with error bars representing the maximal and minimal values within the triplicate sets.

Fluorescence Microscopy. Wide-field fluorescence microscopy of protein aggregates was performed according to ref *15*.

RESULTS

Time traces of aggregation were measured for 100 μM protein solutions in 25 mM Tris-HCl, pH 7.5, without any additions or with addition of either 150 mM NaCl, 0.3 mM spermine, 3 mM spermine, or 10 mM $MgCl_2$. Measurements were also performed in 50 mM Na-acetate, pH 4.0. The aggregation process was generally followed in triplicate by measuring ThioT fluorescence of aliquots removed from the protein incubations. The time traces and individual fits for all incubations, i.e., constructs/conditions, as well as the average fits referred to in the following discussion, are shown in Figure S1 of the Supporting Information. In the majority of cases, the increase of ThioT fluorescence was accompanied by the emergence of visible turbidity. For several samples, static light scattering, a measure of particle formation, was recorded in addition to ThioT fluorescence, which is regarded as an amyloid specific probe. In general, light scattering and ThioT fluorescence increased in parallel, supporting the view that both techniques probe the same process, i.e., amyloid formation (see data for 25 mM Tris-HCl, pH 7.5, 150 mM NaCl in Figure S1). An exception to this was observed for the aggregation of the full-length proteins in the presence of 10 mM $MgCl_2$, in which the appearance of ThioT fluorescence was retarded in comparison to light scattering, suggesting that large amorphous aggregates formed initially and converted slowly into structures exhibiting stronger ThioT binding. In these cases the average aggregation time traces were calculated from the light scattering data.

The aggregation half-times ($t_{1/2}$, incubation time required for ThioT fluorescence or light scattering to reach 50% of the final intensity) for all investigated proteins and conditions are given in Figure 2. A global evaluation of all construct/condition combinations revealed a strong correlation between

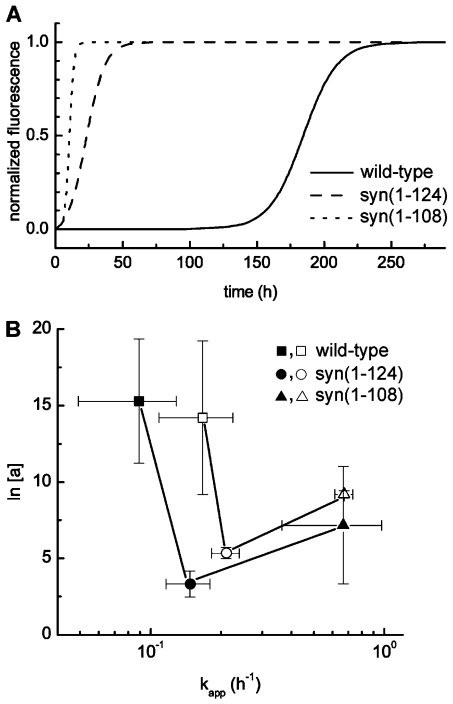

FIGURE 3: Aggregation kinetics of wild-type α-synuclein and the C-terminally truncated variants. (A) Averaged fits and (B) derived parameters of ThioT fluorescence time traces obtained from triplicate incubations of 100 μM protein in 25 mM Tris-HCl, pH 7.5, in the absence of any further additions (A and B, filled symbols) or in the presence of 150 mM NaCl (B, open symbols). (B) Fit constant *a*, reflecting nucleation propensity, plotted versus the aggregation growth rate k_{app}. The data points for the three constructs are connected for clarity. Errors in SD units.

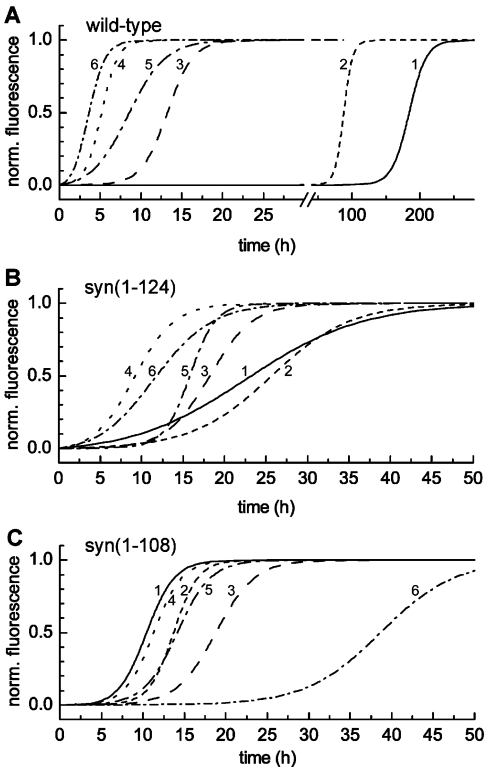

FIGURE 4: Dependence on solution conditions of the aggregation kinetics of wild-type α-synuclein and the C-terminally truncated variants. Solution conditions: (1−5) 25 mM Tris-HCl, pH 7.5, (1) without additions or in the presence of (2) 150 mM NaCl, (3) 10 mM $MgCl_2$, (4) 0.3 mM spermine, (5) 3 mM spermine, or (6) 50 mM Na-acetate, pH 4.0. Averaged fits of ThioT fluorescence/static light scattering time traces obtained from triplicate incubations of 100 μM protein.

$t_{1/2}$ and both the propensity for nucleation, reflected by the fit constant *a* and the rate of aggregate growth, obtained as the fit constant k_{app} (Figure S2 of Supporting Information). These features imply interesting relationships between the underlying thermodynamic and kinetic parameters defining the aggregation mechanism. We anticipate that current efforts directed at the development of more precise, multiparametric association−aggregation assays will yield the quality of data required for detailed interpretations. Presently, $t_{1/2}$ constitutes a useful and fairly robust index of the overall aggregation propensity corresponding to a specific combination of protein structure and solution condition.

Differential Aggregation Kinetics of Full-Length and C-Terminally Truncated α-Synuclein Depending on Solution Conditions. The aggregation time-traces of full-length wild-type α-synuclein and the C-terminally truncated variants syn(1−124) and syn(1−108) in 25 mM Tris, pH 7.5, without addition of further compounds, are shown in Figure 3A. Truncation of the C-terminal 16 amino acid residues of the full-length protein, producing syn(1−124), resulted in an approximately 8-fold reduction of $t_{1/2}$ from ∼180 h to ∼23 h. Additional truncation of the next 16 C-terminal amino acid residues, yielding syn(1−108), involved a further but less pronounced decrease in $t_{1/2}$ from ∼23 h to ∼10 h. Comparison of the propensities for nucleation and aggregate growth, characterized by the respective values of *a* and k_{app}, reveals that the truncation of aa125−140 mainly entailed facilitated nucleation, whereas further truncation of aa109−124 did not further promote nucleation but mainly accelerated aggregate growth (Figure 3B).

The aggregation kinetics of the full-length protein and the C-terminally truncated variants were modulated in unequal ways by changes in the solution conditions (Figure 4). For full-length wild-type α-synuclein, addition of 150 mM NaCl led to faster aggregation with a decrease in $t_{1/2}$ by a factor of ∼2. In contrast, $t_{1/2}$ slightly increased for both syn(1−124) and syn(1−108). However, the order wt > syn(1−124) > syn(1−108) for the magnitude of $t_{1/2}$ was still valid in the presence of 150 mM NaCl. Moreover, the importance of aa125−140 for the slow nucleation of the full-length protein was still manifest (Figure 3B).

Addition of 0.3 mM of the biogenic polyamine spermine led to a reversed order of the $t_{1/2}$ values, syn(1−108) > syn(1−124) > wt. Aggregation of the full-length protein was strongly promoted under these conditions, with a ∼35-fold reduction of $t_{1/2}$. Similarly, the presence of 0.3 mM spermine accelerated syn(1−124) aggregation but with a less pronounced effect compared to the full-length protein. Syn(1−108) aggregation was virtually unaffected by the presence of 0.3 mM spermine.

The K_D of spermine binding to α-synuclein was determined by NMR as 0.61 ± 0.03 mM at 15 °C (*14*). On the basis of this binding constant, full-length α-synuclein would be saturated to ∼30% in the presence of 0.3 mM spermine at a protein concentration of 100 μM. To investigate the aggregation kinetics at higher saturation, the experiments were repeated in the presence of 3 mM spermine, yielding a saturation of ∼83% for full-length α-synuclein. Inasmuch as the K_D was derived from NMR experiments carried out

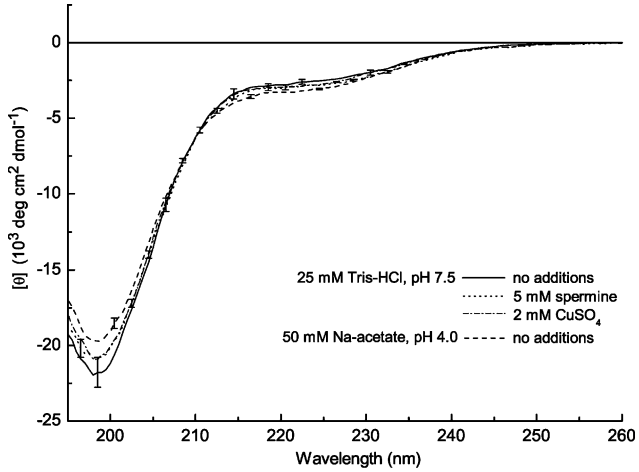

FIGURE 5: Natively unfolded CD spectrum retained for monomeric α-synuclein under conditions linked to C-terminal charge shielding. Far-UV CD spectra of α-synuclein (78 μM). Measurements were done in triplicates with the error bars representing the standard deviation.

at 15 °C and in the presence of 100 mM NaCl, the actual saturation values in the present study might have deviated somewhat from the calculated values given above. Interestingly, 3 mM spermine was less effective in promoting the aggregation of both full-length α-synuclein and syn(1−124) compared to 0.3 mM spermine. In contrast to 0.3 mM spermine, 3 mM spermine had a perceptible effect on aggregation of syn(1−108) with slower aggregation in the presence of the polyamine.

As in the presence of polyamines, the aggregation of full-length α-synuclein was strongly promoted when 10 mM $MgCl_2$ was added to the incubations. For syn(1−124), $t_{1/2}$ decreased slightly upon addition of 10 mM $MgCl_2$, whereas it increased approximately 2-fold for syn(1−108). Decreasing the incubation pH to 4.0 resulted in accelerated aggregation of the full-length protein and syn(1−124), with a distinctly stronger effect for the full-length protein. Aggregation of syn(1−108) was decidedly retarded at pH 4.0, with a $t_{1/2} \sim$ 40 h compared to ∼10 h at pH 7.5.

The enhancement of aggregation of full-length α-synuclein by spermine or $MgCl_2$ addition was not associated with secondary structure changes for the monomeric protein detectable by CD spectroscopy (Figure 5), i.e., the CD spectrum remained indicative of the natively unfolded nature of the protein. The CD changes were within the error of the measurement for addition of spermine at saturating concentrations, as well as in the presence of Mg^{2+} or Cu^{2+}; the latter ion is reportedly one of the most effective in the promotion of α-synuclein aggregation (*17*, *18*). Decreasing the pH to 4.0 resulted in an increase in ellipticity in the region around 200 nm and a decrease around 220 nm, although these effects were very small and exceeded the measurement error only slightly.

Aggregate Morphologies of Full-Length and C-Terminally Truncated Variants. The final turbidity in the postaggregation steady state for the different constructs/conditions is given in Figure 6. The full-length α-synucleins, wild-type, A30P, and A53T, exhibited very similar turbidities, but varied with respect to the different solution conditions. In 25 mM Tris-HCl, pH 7.5, without further additions, the solutions appeared transparent, whereas in the presence of 150 mM NaCl visible

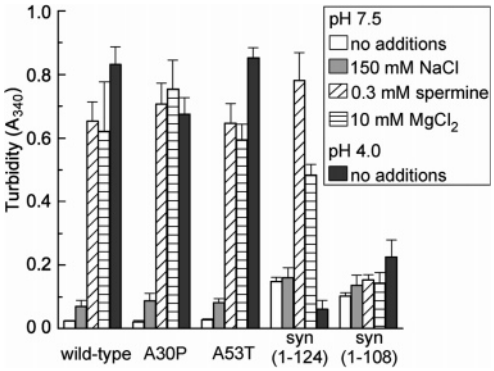

FIGURE 6: Dependence on solution conditions of the aggregation morphology of the full-length α-synucleins and the C-terminally truncated variants. Final turbidity (A_{340}) of the 100 μM protein incubations. The aggregate solutions were diluted 8.5-fold before reading of A_{340}. Errors in SD units.

turbidity was generated. In the spermine- or $MgCl_2$-containing samples as well as in 50 mM Na-acetate, pH 4.0, large particles were formed that produced strong turbidity. The turbidity profiles of syn(1−124) and syn(1−108) were different from that of the full-length proteins. Both truncation mutants exhibited visible turbidity in 25 mM Tris, pH 7.5, without further additions, and addition of 150 mM NaCl had no obvious effect. Addition of spermine or $MgCl_2$ to syn(1−124) incubations resulted in increased turbidity, whereas aggregation of this variant at pH 4.0 led to a lower turbidity compared to pH 7.5. In the case of syn(1−108), little changes in turbidity upon addition of spermine or salts were detected. At pH 4.0, syn(1−108) solutions achieved slightly higher turbidity values compared to pH 7.5 incubations.

The observed turbidities were reflected in electron microscopy (EM) and fluorescence microscopy images of the aggregate structures. Mature amyloid fibrils ∼10 nm in diameter and several micrometers in length were found in electron micrographs from the transparent solutions of full-length α-synuclein at pH 7.5 without additions (Figure 7A). Fluorescence microscopy of these solutions in the presence of ThioT did not reveal any defined structures but showed a faint background fluorescence of ThioT, indicating that the fibrils were uniformly distributed in the solution. In contrast, in the case of the C-terminally truncated proteins the ThioT fluorescence was localized in discrete spots with dimensions of a few hundred micrometers (Figure S3A of Supporting Information). The ability of syn(1−124) and syn(1−108) to form fibrils of similar morphology as the full-length protein was evidenced by EM (Figure 7B,C). However, these fibrils were shorter and possessed a higher tendency to associate, resulting in bundles of fibrils and probably large fibril networks that could be detected by fluorescence microscopy.

As in the case of C-terminal truncation, the presence of 150 mM NaCl resulted in a shift toward shorter fibrils with a higher association tendency (Figure 7D). The ThioT fluorescence originating from these aggregates was localized in extended, diffuse areas (Figure S3B). Under the conditions linked to the highest turbidity levels, i.e., at pH 7.5 in the presence of spermine or $MgCl_2$ or at pH 4, full-length α-synuclein was incorporated into large particles visible as discrete spots by fluorescence microscopy (Figure S3C). It was reported before that these aggregates frequently have an amorphous appearance, although they share characteristics typical of amyloid (*15*, *21*).

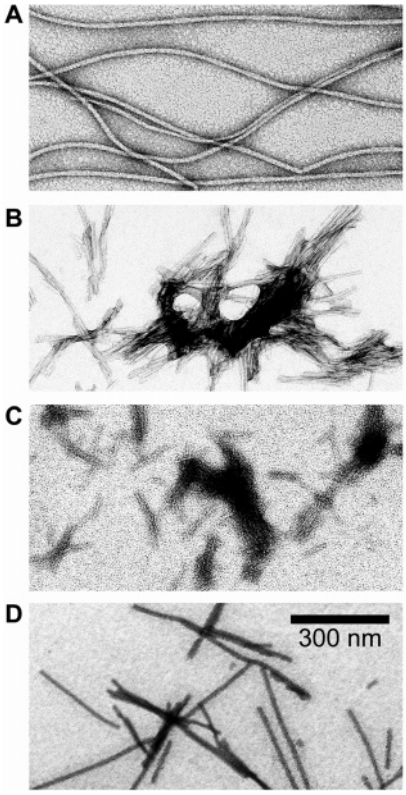

FIGURE 7: Electron microscopy of fibrils formed from (A, D) wild-type α-synuclein, (B) syn(1−124), and (C) syn(1−108). Incubation conditions: 100 μM protein in (A−C) 25 mM Tris-HCl, pH 7.5, or (D) 25 mM Tris-HCl, pH 7.5, 150 mM NaCl.

The Effects of the Disease-Related Mutations on the Aggregation Kinetics Depend on Solution Conditions. Figure 8 shows the aggregation time traces of the full-length proteins wild-type, A53T and A30P. At pH 7.5, in the absence of further additions, wild-type and A53T aggregation occurred with a similar $t_{1/2}$ (Figure 8A). In contrast, the aggregation of A30P was significantly retarded. Thus, the order of aggregation propensity was wt ∼ A53T > A30P under this condition. The presence of 150 mM NaCl promoted the aggregation of all proteins, although to a different extent (Figure 8B). A53T aggregated distinctly faster than the wild-type, resulting in the aggregation propensity order A53T > wt > A30P.

For all other conditions tested in this study, the time traces of the wild-type protein and the A30P mutant were similar, whereas the A53T mutant aggregated faster, i.e., the aggregation propensity order was A53T > wt ∼ A30P (Figure 8C−F). A53T aggregation was particularly enhanced in the presence of spermine, with $t_{1/2}$ reduced by a factor of ∼3.5 for 0.3 mM spermine compared to the wild-type and A30P.

DISCUSSION

The Impact of the C-Terminus on Aggregation Kinetics. Truncation of the 16 or 32 C-terminal amino acid residues of wild-type α-synuclein resulted in a pronounced acceleration of aggregation. A striking feature of the truncated region is its high density of acidic residues, with four aspartate and eight glutamate residues in aa109−140, whereas basic amino acids are absent. Thus, electrostatic effects likely account for the different aggregation properties of the full-length protein and its truncated variants. In fact, the charge state of amyloidogenic proteins/peptides constitutes a major determinant of their aggregation rate (*47*−*49*). Chiti et al. investigated the aggregation properties of a series of muscle acylphosphatase mutants that implied a change in the net charge of the protein and identified the net charge as a key factor for aggregation, with higher net charge linked to slower aggregation (*47*). The aggregation rates correlated better with the net charge than with the charge state of regions implicated in nucleation. Moreover, mutations outside of these regions were identified that modified the aggregation kinetics. These observations suggest that the effects of charge changes on aggregation, in contrast to those caused by changes in hydrophobicity and β-sheet propensity, are not confined to local regions but arise from a modulation of an overall property of the protein, i.e., the net charge (*47*, *48*, *50*). This view is further supported by the increased tendency of amyloidogenic proteins/peptides for amyloid formation at pH values near their isoelectric point (pI), where their net charge is zero (*49*, *51*). The importance of the net charge for amyloid aggregation presumably derives from its role as a determinant of the strength of electrostatic repulsion between molecules undergoing self-assembly.

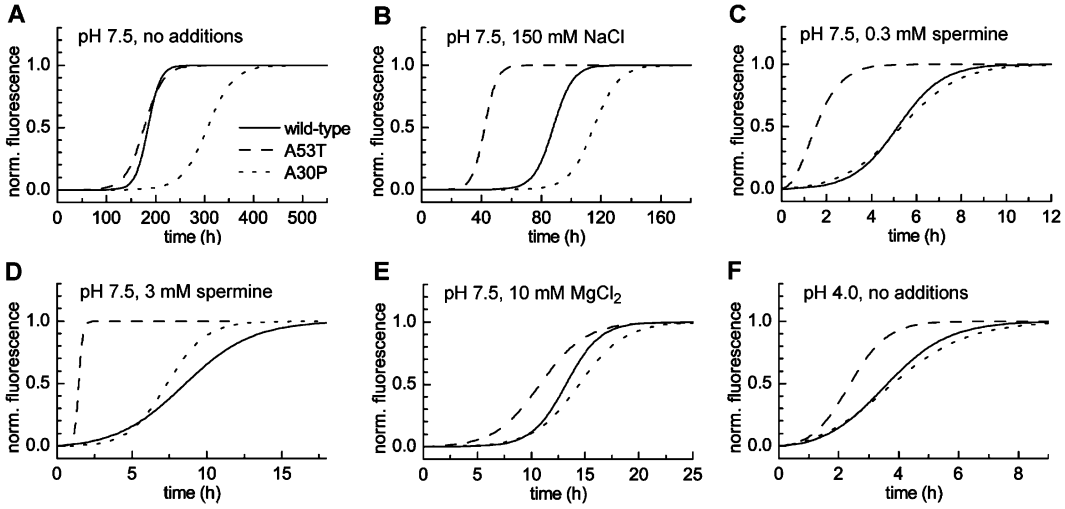

FIGURE 8: Dependence on solution conditions of the aggregation kinetics of wild-type α-synuclein and the disease-related mutants A53T and A30P. Averaged fits of ThioT fluorescence/static light scattering time traces obtained from triplicate incubations of 100 μM protein.

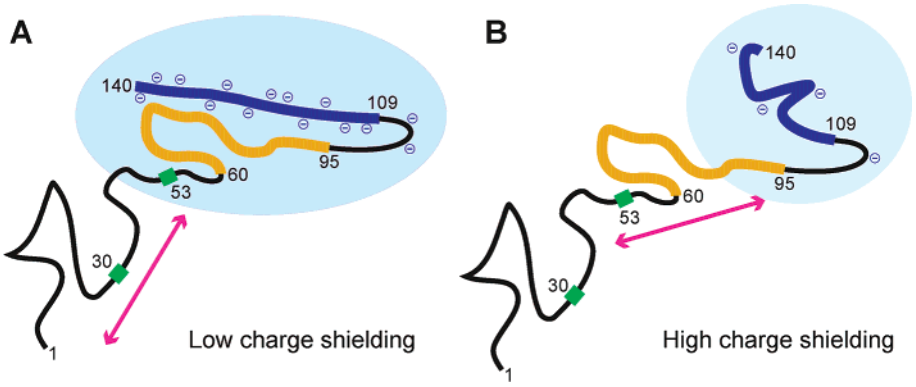

FIGURE 9: Schematic model of a possible mechanism of interplay between the C-terminus and the central/N-terminal parts of α-synuclein. (A) Under low charge shielding conditions, the C-terminus (region aa109−140 in blue) possesses a high density of negative charges, resulting in a preferential population of extended conformations and screening of the regions exhibiting the highest propensity for amyloid formation (NAC region in orange). (B) Under high charge shielding conditions, the C-terminus is compacted and less charged, entailing less efficient screening of the amyloidogenic regions. Magenta arrows, a rough indication of the sequence regions determining the speed of aggregation, accounting for the dependence of the effects of the disease-related mutations (green) on the state of C-terminal charge shielding.

Table 1: Net Charges of Full-Length and Truncated α-Synuclein at the pH Values Applied in This Work[a]

	pH 7.5	pH 4.0
full-length α-synuclein	−9.0	+4.4
syn(1−124)	−3.0	+7.2
syn(1−108)	+3.0	+10.3

[a] Calculated using pK_a values from ref *45*.

Several observations in this study can be explained with the overall electrostatic states of the proteins involved: (i) Truncation of the 16 or 32 C-terminal amino acid residues of full-length α-synuclein, resulting in a reduction of absolute net charge from 9 to 3 at pH 7.5 (Table 1), led to accelerated aggregation either without additions or in the presence of 150 mM NaCl. (ii) Shielding of the negative charges in the full-length protein by monovalent Na^+, divalent Mg^{2+}, or polycationic polyamines promoted aggregation of full-length α-synuclein. (iii) Lowering the pH to 4.0, a value close to the pI of α-synuclein (4.4), increased the aggregation rate of the full-length protein dramatically. (iv) At pH 4.0, the ranking of the protein constructs with respect to their aggregation propensity was full-length > syn(1−124) > syn(1−108), paralleling that for smaller net charge (Table 1).

However, some observations contradict the notion of exclusively global, sequence-unspecific electrostatic effects: (i) syn(1−124) and syn(1−108) have the same absolute net charge at pH 7.5, but syn(1−124) exhibited a decidedly slower aggregation than syn(1−108) with or without 150 mM NaCl. (ii) The absolute net charge of syn(1−124) is distinctly higher at pH 4.0 than at pH 7.5 (net charge +7.2 and −3.0, respectively; Table 1), but aggregation occurred more slowly at pH 7.5, with a ∼2-fold longer $t_{1/2}$. (iii) At pH 4.0, syn(1−108) has the highest net charge (+10.3) of all constructs/conditions employed in this study; however, the full-length protein at pH 7.5 (net charge −9.0) aggregated more slowly with a ∼5-fold greater $t_{1/2}$. In all these cases, the slower aggregation correlated with a high density of negative charges in the regions aa109−124 or aa109−140, suggesting that the C-terminus exerts specific effects on aggregation in addition to its contribution to the overall charge. This conclusion is supported by a recent study of the heat-induced aggregation of fusion proteins incorporating α-synuclein C-terminal-derived peptides (*52*).

At pH 7.5 in buffer with or without 150 mM NaCl, successive truncation of the two acidic repeats in the C-terminus had unequal influences on the nucleation and the growth processes. The presence of the second acidic repeat, i.e., the entirety of the C-terminus, was required for the slow nucleation observed for the full-length protein. This effect could be explained on the basis of simple electrostatic considerations, assuming that at low or moderate ionic strength the flexible protein chain preferentially adopts conformations in which the negatively charged C-terminus is in close proximity to the regions involved in β-sheet formation, represented primarily by the highly hydrophobic central region (residues 60−95) (*29*, *30*) as well as by the parts of the N-terminus incorporated into the fibril core (residues ∼30−59) (*40*, *41*) (Figure 9A). In such a situation, the negatively charged C-termini of monomers could impede the encounter and association of the aggregation-prone regions by charge−charge repulsion. Recent NMR experiments based on two-dimensional $^1H-^{15}N$ HSQC spectroscopy of backbone amides (*14*) and dipolar couplings and paramagnetic relaxation enhancement (Bertoncini, C. W., Jung, Y.-S., Fernández, C. O., Hoyer, W., Griesinger, C., Jovin, T. M., Zweckstetter, M., unpublished experiments) have detected long-range interactions in monomeric α-synuclein, suggesting that a hydrophobic cluster comprising the C-terminal part of the highly hydrophobic NAC region (residues 85−95) and the C-terminus (residues 110−130) provides the structural basis for the autoinhibition of α-synuclein aggregation. The masking of an aggregation-prone domain by the C-terminus is also consistent with the conclusions derived from in vivo studies of alternative splice forms of rodent α-synuclein (*53*). Possibly, interactions of the C-terminus with the central region are facilitated when the C-terminus preferentially adopts extended conformations, thereby spanning the amyloidogenic regions. Extended conformations of the C-terminus might be favored as a consequence of intramolecular charge repulsion caused by the high density of negative charges.

In the context of the suggested model, shielding of negative charges by addition of Na^+, Mg^{2+}, or polyamines or

decreased pH would result in (a) a reduced charge and (b) compaction of the C-terminus. Both effects would reduce its inhibitory function on self-aggregation of the amyloidogenic region, thus leading to the observed acceleration of aggregation (Figure 9B).

Addition of 0.3 mM spermine exhibited no significant effect on the aggregation kinetics of syn(1−108), reconfirming that aa109−140 is the polyamine binding site (*14*). The promotion of aggregation by 0.3 mM spermine therefore reflects binding to aa109−140. Full-length α-synuclein aggegrated faster in the presence of 0.3 mM spermine than the truncated variants under all conditions, from which we conclude that the effect of polyamine binding is not only an overrriding of the inhibition exerted by the C-terminus. The mechanism underlying the additional facilitation of aggregation is as yet unclear; bridging of protein monomers by the multivalent polyamine is one of many possibilities.

The effects of 3 mM spermine and 10 mM $MgCl_2$ on full-length α-synuclein and syn(1−124) cannot be exclusively assigned to altered properties of the C-terminus, since under these conditions syn(1−108) aggregation kinetics was modulated as well. However, the effects on syn(1−108) were only minor and, more importantly, reversed, i.e., with slower aggregation in the presence of the additions. Thus, the accelerating effect on aggregation can be attributed to interaction of cationic substances with the C-terminus in these cases as well. These findings show that Mg^{2+} as well as the polyamines promotes aggregation by binding to aa109−140, a conclusion that is likely to prove valid for other metal ions as well; for example, α-synuclein undergoes oligomerization upon Ca^{2+}- or Cu^{2+}-binding to the C-terminus (*18*, *19*). The results presented here demonstrate that the presence of a single acidic repeat suffices for the interaction of polyamines and metal ions with the C-terminus of α-synuclein, inasmuch as syn(1−124) aggregation was significantly accelerated by these compounds.

In contrast to spermine addition, the reduction of pH to 4.0 exerted a strong impact on syn(1−108) aggregation, presumably reflecting the effect of pH change on the net charge of the protein and also highlighting the specificity of the polyamine interaction.

The CD spectra of monomeric wild-type α-synuclein were virtually identical for all conditions employed in this study, indicating that C-terminal charge shielding did not induce a major change in secondary structure, a finding consistent with the unaltered C^{α} shifts in NMR in the presence of polyamines (*14*). We conclude that the population of a partially folded intermediate, proposed previously for conditions of decreased pH or presence of metal ions (*16*, *17*), is unlikely to account for the enhancement of aggregation under the conditions employed in this study. A facilitated formation of a partially folded intermediate under high charge shielding conditions is not required in a model such as that presented in Figure 9, supposing that the C-terminal charge state exerts its impact by regulating the contact probability between the amyloidogenic regions of two (or more) monomers.

Aggregation Acceleration by the A53T Mutation Is Connected to C-Terminal Charge Shielding. Surprisingly, the aggregation kinetics of wild-type α-synuclein, A30P, and A53T were modulated differently by changes of the solution conditions. At pH 7.5 in the presence of 150 mM NaCl, conditions similar to those typically employed in the literature on α-synuclein aggregation kinetics, the order of aggregation propensity was A53T > wt > A30P, in agreement with the results obtained for total aggregation by two other groups (*23*, *42*, *44*). At lower ionic strength (without addition of 150 mM NaCl) the order was wt ∼ A53T > A30P, whereas with high charge shielding in the C-terminus (addition of polyamines, Mg^{2+}, pH 4.0) it was A53T > wt ∼ A30P. These findings could also be accounted for by the previously suggested model proposing an interaction of the C-terminus with the central and N-terminal parts (Figure 9), assuming the following: (i) different regions in the α-synuclein sequence vary in their propensity for self-association, with that of the region about residue 53 greater than that exhibited by the region around residue 30. (ii) The aggregation propensity is increased by the A53T mutation but reduced by the A30P mutation, a notion consistent with the predisposition of the involved amino acids for forming *β*-sheets (*54*). At low ionic strength, the intramolecular charge−charge repulsion and, as a consequence, the average extension of the C-terminus would be maximal, possibly resulting in the shielding of the central part as well as the region including residue 53. In this situation, the aggregate formation might originate from sequence regions positioned closer to the N-terminus such as that enclosing residue 30, entailing a sensitivity of the aggregation kinetics to the A30P mutation, whereas the A53T mutation would be ineffective. In contrast, high charge shielding would be accompanied by a compaction of the C-terminus and less potent shielding of the region comprising residue 53, resulting in a faster aggregation with sensitivity to the A53T mutation. The A30P mutant would be without effect due to its location in a sequence region that is not limiting the rate of aggregation under these conditions.

The C-Terminus Accounts for Morphological Diversity of α-Synuclein Aggregates. The turbidity of full-length α-synuclein aggregates depended dramatically on incubation conditions, reflecting the high diversity of aggregate morphology (*15*). The morphological diversity originates from the C-terminus (residues 109−140), since the turbidity of syn(1−108) incubations was affected only marginally and can be explained by the high variability of the charge state of the fibril surfaces, taking into account that the C-terminus is present on these surfaces (*39*−*41*). Low ionic strength results in a high density of negative charges present on the fibril surfaces, leading to strong charge−charge repulsion between individual fibrils and thus reduced interfibrillar contacts. Strong charge shielding weakens the charge−charge repulsions between fibrils and thereby increases the probability of interfibrillar association, eventually leading to large aggregates of amorphous appearance. In the presence of Mg^{2+} and spermine, an additional bridging function of the multivalent cations that drives the formation of large fibril assemblies is conceivable.

In contrast to the truncated variants, fast aggregation correlated with high final turbidity for the full-length proteins, suggesting a link between aggregation kinetics and aggregate morphology that is mediated by the C-terminus. This finding points to an active role of the fibril surfaces in the aggregation process rather than exclusively determining the degree of interfibrillar association. The facilitated formation of new nuclei on the surface of existing fibrils and unspecific deposition of protein on these surfaces constitute two possible

mechanisms. In fact, we recently observed the growth of aggregates of amorphous appearance from the surfaces of initially formed fibrils at pH 5.0 by in situ atomic force microscopy (*26*). The accessibility of such alternative aggregation mechanisms acting in addition to strictly fibril-extension might, in combination with subtle changes in the conformational space covered by the protein monomer that modulate its nucleation/aggregation propensity, determine the observed aggregation kinetics for each construct/condition pair.

In this respect, the acidic C-terminal region aa109−140 constitutes a key domain that regulates the properties of α-synuclein both in its monomeric and aggregated forms. Further experiments are being performed to gain a better understanding of the interplay between the C-terminus and the remainder of the molecule. Preferential long-range interactions in the natively unfolded protein would be informative from a structural as well as a biomedical perspective. The extent of charge shielding of C-terminal amino acid residues in vivo and its possible alteration in disease is as yet unknown. Nevertheless, the present study demonstrates that the aggregation kinetics are sensitive to a wide range of ionic conditions, from weak C-terminal charge shielding (absence of additions) to medium (150 mM NaCl) and strong charge shielding (e.g., in the presence of polyamines). Thus, relatively modest alterations in ionic conditions may affect the aggregation behavior. (Poly)cations such as polyamines (*55*) and metal ions (*56*, *57*) have been implicated in PD and might exert neurotoxic effects by promoting α-synuclein aggregation as a consequence of C-terminal charge shielding.

ACKNOWLEDGMENT

We acknowledge fruitful discussions with our colleagues C. Bertoncini, C.O. Fernández, C. Griesinger, E.A. Jares-Erijman, R. Klement, R.J. Vermeij, and M. Zweckstetter. We are indebted to H. Urlaub for performing the ESI-MS measurements and to A. Dichter for valuable technical assistance.

SUPPORTING INFORMATION AVAILABLE

Original data and fits of the aggregation kinetics (Figure S1), global analysis of the fit parameters (Figure S2) for all constructs/conditions, and fluorescence microscopy images of α-synuclein aggregates (Figure S3). This material is available free of charge via the Internet at http://pubs.acs.org.

REFERENCES

1. Goedert, M. (2001) Alpha-synuclein and neurodegenerative diseases, *Nat. Rev. Neurosci. 2*, 492−501.
2. Dev, K. K., Hofele, K., Barbieri, S., Buchman, V. L., and van der Putten, H. (2003) Part II: α-Synuclein and its molecular pathophysiological role in neurodegenerative disease, *Neuropharmacology 45*, 14−44.
3. Spillantini, M. G., Schmidt, M. L., Lee, V. M., Trojanowski, J. Q., Jakes, R., and Goedert, M. (1997) α-Synuclein in Lewy bodies, *Nature 388*, 839−840.
4. Baba, M., Nakajo, S., Tu, P. H., Tomita, T., Nakaya, K., Lee, V. M., Trojanowski, J. Q., and Iwatsubo, T. (1998) Aggregation of alpha-synuclein in Lewy bodies of sporadic Parkinson's disease and dementia with Lewy bodies, *Am. J. Pathol. 152*, 879−884.
5. Wakabayashi, K., Yoshimoto, M., Tsuji, S., and Takahashi, H. (1998) α-Synuclein immunoreactivity in glial cytoplasmic inclusions in multiple system atrophy, *Neurosci. Lett. 249*, 180−182.
6. Kruger, R., Kuhn, W., Muller, T., Woitalla, D., Graeber, M., Kosel, S., Przuntek, H., Epplen, J. T., Schols, L., and Riess, O. (1998) Ala30Pro mutation in the gene encoding alpha-synuclein in Parkinson's disease, *Nat. Genet. 18*, 106−108.
7. Polymeropoulos, M. H., Lavedan, C., Leroy, E., Ide, S. E., Dehejia, A., Dutra, A., Pike, B., Root, H., Rubenstein, J., Boyer, R., Stenroos, E. S., Chandrasekharappa, S., Athanassiadou, A., Papapetropoulos, T., Johnson, W. G., Lazzarini, A. M., Duvoisin, R. C., Di Iorio, G., Golbe, L. I., and Nussbaum, R. L. (1997) Mutation in the α-synuclein gene identified in families with Parkinson's disease, *Science 276*, 2045−2047.
8. Weinreb, P. H., Zhen, W., Poon, A. W., Conway, K. A., and Lansbury, P. T., Jr. (1996) NACP, a protein implicated in Alzheimer's disease and learning, is natively unfolded, *Biochemistry 35*, 13709−13715.
9. Hashimoto, M., Hsu, L. J., Sisk, A., Xia, Y., Takeda, A., Sundsmo, M., and Masliah, E. (1998) Human recombinant NACP/α-synuclein is aggregated and fibrillated in vitro: Relevance for Lewy body disease, *Brain. Res. 799*, 301−306.
10. Giasson, B. I., Uryu, K., Trojanowski, J. Q., and Lee, V. M. (1999) Mutant and wild-type human α-synucleins assemble into elongated filaments with distinct morphologies in vitro, *J. Biol. Chem. 274*, 7619−7622.
11. Serpell, L. C., Berriman, J., Jakes, R., Goedert, M., and Crowther, R. A. (2000) Fiber diffraction of synthetic α-synuclein filaments shows amyloid-like cross-β conformation, *Proc. Natl. Acad. Sci. U.S.A. 97*, 4897−4902.
12. Conway, K. A., Harper, J. D., and Lansbury, P. T., Jr. (2000) Fibrils formed in vitro from α-synuclein and two mutant forms linked to Parkinson's disease are typical amyloid, *Biochemistry 39*, 2552−2563.
13. Wood, S. J., Wypych, J., Steavenson, S., Louis, J. C., Citron, M., and Biere, A. L. (1999) α-Synuclein fibrillogenesis is nucleation-dependent. Implications for the pathogenesis of Parkinson's disease, *J. Biol. Chem. 274*, 19509−19512.
14. Fernández, C. O., Hoyer, W., Zweckstetter, M., Jares-Erijman, E. A., Subramaniam, V., Griesinger, C., and Jovin, T. M. (2004) NMR of α-synuclein-polyamine complexes elucidates the mechanism and kinetics of induced aggregation, *EMBO J. 23*, 2039−2046.
15. Hoyer, W., Antony, T., Cherny, D., Heim, G., Jovin, T. M., and Subramaniam, V. (2002) Dependence of α-synuclein aggregate morphology on solution conditions, *J. Mol. Biol. 322*, 383−393.
16. Uversky, V. N., Li, J., and Fink, A. L. (2001) Evidence for a partially folded intermediate in α-synuclein fibril formation, *J. Biol. Chem. 276*, 10737−10744.
17. Uversky, V. N., Li, J., and Fink, A. L. (2001) Metal-triggered structural transformations, aggregation, and fibrillation of human α-synuclein, *J. Biol. Chem. 276*, 44284−44296.
18. Paik, S. R., Shin, H. J., Lee, J. H., Chang, C. S., and Kim, J. (1999) Copper(II)-induced self-oligomerization of α-synuclein, *Biochem. J. 340*, 821−828.
19. Nielsen, M. S., Vorum, H., Lindersson, E., and Jensen, P. H. (2001) Ca^{2+} binding to α-synuclein regulates ligand binding and oligomerization, *J. Biol. Chem. 276*, 22680−22684.
20. Kim, T. D., Paik, S. R., Yang, C. H., and Kim, J. (2000) Structural changes in α-synuclein affect its chaperone-like activity in vitro, *Protein. Sci. 9*, 2489−2496.
21. Antony, T., Hoyer, W., Cherny, D., Heim, G., Jovin, T. M., and Subramaniam, V. (2003) Cellular polyamines promote the aggregation of α-synuclein, *J. Biol. Chem. 278*, 3235−3240.
22. Goers, J., Uversky, V. N., and Fink, A. L. (2003) Polycation-induced oligomerization and accelerated fibrillation of human α-synuclein in vitro, *Protein. Sci. 12*, 702−707.
23. Conway, K. A., Lee, S. J., Rochet, J. C., Ding, T. T., Williamson, R. E., and Lansbury, P. T., Jr. (2000) Acceleration of oligomerization, not fibrillization, is a shared property of both α-synuclein mutations linked to early-onset Parkinson's disease: Implications for pathogenesis and therapy, *Proc. Natl. Acad. Sci. U.S.A. 97*, 571−576.
24. Ding, T. T., Lee, S. J., Rochet, J. C., and Lansbury, P. T., Jr. (2002) Annular α-synuclein protofibrils are produced when spherical protofibrils are incubated in solution or bound to brain-derived membranes, *Biochemistry 41*, 10209−10217.
25. Lashuel, H. A., Petre, B. M., Wall, J., Simon, M., Nowak, R. J., Walz, T., and Lansbury, P. T., Jr. (2002) α-Synuclein, especially the Parkinson's disease-associated mutants, forms pore-like annular and tubular protofibrils, *J. Mol. Biol. 322*, 1089−1102.

26. Hoyer, W., Cherny, D., Subramaniam, V., and Jovin, T. M. (2004) Rapid self-assembly of α-synuclein observed by in situ atomic force microscopy, *J. Mol. Biol. 340*, 127−139.
27. Chandra, S., Chen, X., Rizo, J., Jahn, R., and Sudhof, T. C. (2003) A broken α-helix in folded α-synuclein, *J. Biol. Chem. 278*, 15313−15318.
28. Bussell, R., Jr., and Eliezer, D. (2003) A structural and functional role for 11-mer repeats in α-synuclein and other exchangeable lipid binding proteins, *J. Mol. Biol. 329*, 763−778.
29. Giasson, B. I., Murray, I. V., Trojanowski, J. Q., and Lee, V. M. (2001) A hydrophobic stretch of 12 amino acid residues in the middle of α-synuclein is essential for filament assembly, *J. Biol. Chem. 276*, 2380−2386.
30. Du, H. N., Tang, L., Luo, X. Y., Li, H. T., Hu, J., Zhou, J. W., and Hu, H. Y. (2003) A peptide motif consisting of glycine, alanine, and valine is required for the fibrillization and cytotoxicity of human α-synuclein, *Biochemistry 42*, 8870−8878.
31. Park, S. M., Jung, H. Y., Chung, K. C., Rhim, H., Park, J. H., and Kim, J. (2002) Stress-induced aggregation profiles of GST-α-synuclein fusion proteins: Role of the C-terminal acidic tail of α-synuclein in protein thermosolubility and stability, *Biochemistry 41*, 4137−4146.
32. Souza, J. M., Giasson, B. I., Lee, V. M., and Ischiropoulos, H. (2000) Chaperone-like activity of synucleins, *FEBS Lett. 474*, 116−119.
33. Park, S. M., Jung, H. Y., Kim, T. D., Park, J. H., Yang, C. H., and Kim, J. (2002) Distinct roles of the N-terminal-binding domain and the C-terminal-solubilizing domain of α-synuclein, a molecular chaperone, *J. Biol. Chem. 277*, 28512−28520.
34. Kim, T. D., Paik, S. R., and Yang, C. H. (2002) Structural and functional implications of C-terminal regions of α-synuclein, *Biochemistry 41*, 13782−13790.
35. Crowther, R. A., Jakes, R., Spillantini, M. G., and Goedert, M. (1998) Synthetic filaments assembled from C-terminally truncated α-synuclein, *FEBS Lett. 436*, 309−312.
36. Murray, I. V., Giasson, B. I., Quinn, S. M., Koppaka, V., Axelsen, P. H., Ischiropoulos, H., Trojanowski, J. Q., and Lee, V. M. (2003) Role of α-synuclein carboxy-terminus on fibril formation in vitro, *Biochemistry 42*, 8530−8540.
37. Fujiwara, H., Hasegawa, M., Dohmae, N., Kawashima, A., Masliah, E., Goldberg, M. S., Shen, J., Takio, K., and Iwatsubo, T. (2002) α-Synuclein is phosphorylated in synucleinopathy lesions, *Nat. Cell. Biol. 4*, 160−164.
38. Giasson, B. I., Duda, J. E., Murray, I. V., Chen, Q., Souza, J. M., Hurtig, H. I., Ischiropoulos, H., Trojanowski, J. Q., and Lee, V. M. (2000) Oxidative damage linked to neurodegeneration by selective α-synuclein nitration in synucleinopathy lesions, *Science 290*, 985−989.
39. Crowther, R. A., Daniel, S. E., and Goedert, M. (2000) Characterisation of isolated α-synuclein filaments from substantia nigra of Parkinson's disease brain, *Neurosci. Lett. 292*, 128−130.
40. Der-Sarkissian, A., Jao, C. C., Chen, J., and Langen, R. (2003) Structural organization of α-synuclein fibrils studied by site-directed spin labeling, *J. Biol. Chem. 278*, 37530−37535.
41. Miake, H., Mizusawa, H., Iwatsubo, T., and Hasegawa, M. (2002) Biochemical characterization of the core structure of α-synuclein filaments, *J. Biol. Chem. 277*, 19213−19219.
42. Conway, K. A., Harper, J. D., and Lansbury, P. T. (1998) Accelerated in vitro fibril formation by a mutant α-synuclein linked to early-onset Parkinson disease, *Nat. Med. 4*, 1318−1320.
43. Narhi, L., Wood, S. J., Steavenson, S., Jiang, Y., Wu, G. M., Anafi, D., Kaufman, S. A., Martin, F., Sitney, K., Denis, P., Louis, J. C., Wypych, J., Biere, A. L., and Citron, M. (1999) Both familial Parkinson's disease mutations accelerate α-synuclein aggregation, *J. Biol. Chem. 274*, 9843−9846.
44. Li, J., Uversky, V. N., and Fink, A. L. (2001) Effect of familial Parkinson's disease point mutations A30P and A53T on the structural properties, aggregation, and fibrillation of human α-synuclein, *Biochemistry 40*, 11604−11613.
45. Dawson, R. M. C., Elliott, D. C., Elliott, W. H., and Jones, K. M. (1986) *Data for biochemical research*, 3rd ed., Oxford Science Publications.
46. Dubochet, J., Ducommun, M., Zollinger, M., and Kellenberger, E. (1971) A new preparation method for dark-field electron microscopy of biomacromolecules, *J. Ultrastruct. Res. 35*, 147−167.
47. Chiti, F., Calamai, M., Taddei, N., Stefani, M., Ramponi, G., and Dobson, C. M. (2002) Studies of the aggregation of mutant proteins in vitro provide insights into the genetics of amyloid diseases, *Proc. Natl. Acad. Sci. U.S.A. 99*, 16419−16426.
48. Chiti, F., Stefani, M., Taddei, N., Ramponi, G., and Dobson, C. M. (2003) Rationalization of the effects of mutations on peptide and protein aggregation rates, *Nature 424*, 805−808.
49. Schmittschmitt, J. P., and Scholtz, J. M. (2003) The role of protein stability, solubility, and net charge in amyloid fibril formation, *Protein Sci. 12*, 2374−2378.
50. Chiti, F., Taddei, N., Baroni, F., Capanni, C., Stefani, M., Ramponi, G., and Dobson, C. M. (2002) Kinetic partitioning of protein folding and aggregation, *Nat. Struct. Biol. 9*, 137−143.
51. Pavlov, N. A., Cherny, D. I., Heim, G., Jovin, T. M., and Subramaniam, V. (2002) Amyloid fibrils from the mammalian protein prothymosin α, *FEBS Lett. 517*, 37−40.
52. Park, S. M., Ahn, K. J., Jung, H. Y., Park, J. H., and Kim, J. (2004) Effects of novel peptides derived from the acidic tail of synuclein (ATS) on the aggregation and stability of fusion proteins, *Protein Eng. Des. Sel. 17*, 251−260.
53. McLean, P. J., and Hyman, B. T. (2002) An alternatively spliced form of rodent α-synuclein forms intracellular inclusions in vitro: Role of the carboxy-terminus in α-synuclein aggregation, *Neurosci. Lett. 323*, 219−223.
54. Chou, P. Y., and Fasman, G. D. (1978) Empirical predictions of protein conformation, *Annu. Rev. Biochem. 47*, 251−276.
55. Gomes-Trolin, C., Nygren, I., Aquilonius, S. M., and Askmark, H. (2002) Increased red blood cell polyamines in ALS and Parkinson's disease, *Exp. Neurol. 177*, 515−520.
56. Lai, B. C., Marion, S. A., Teschke, K., and Tsui, J. K. (2002) Occupational and environmental risk factors for Parkinson's disease, *Parkinsonism Relat. Disord. 8*, 297−309.
57. Wolozin, B., and Golts, N. (2002) Iron and Parkinson's disease, *Neuroscientist 8*, 22−32.

BI048453U